

# ASemConsist: Adaptive Semantic Feature Control for Training-Free Identity-Consistent Generation

Shin Seong Kim<sup>1\*</sup> Minjung Shin<sup>1\*</sup> Hyunin Cho<sup>1</sup> Youngjung Uh<sup>1†</sup>  
Yonsei University<sup>1</sup>

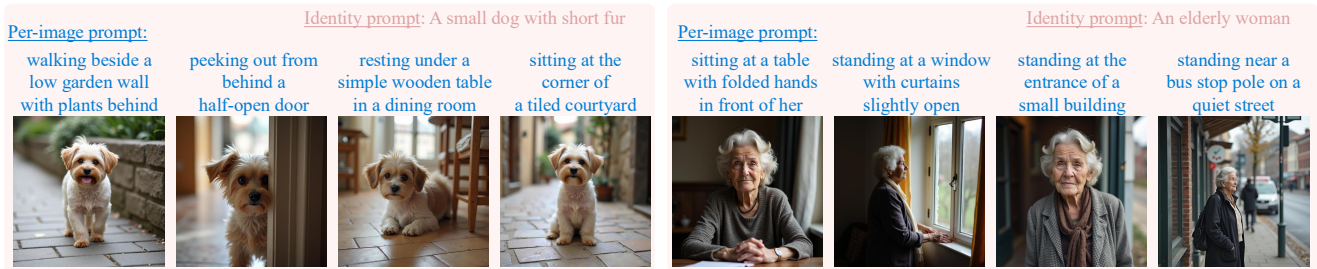


Figure 1. Overview of the consistent story generation task and our results. The identity prompt, provides the shared character description across all images. The per-image descriptions, specify unique attributes for each image. Our results show consistent character representation across images, with each per-image description effectively reflected.

## Abstract

Recent text-to-image diffusion models have significantly improved visual quality and text alignment. However, generating a sequence of images while preserving consistent character identity across diverse scene descriptions remains a challenging task. Existing methods often struggle with a trade-off between maintaining identity consistency and ensuring per-image prompt alignment. In this paper, we introduce a novel framework, ASemconsist, that addresses this challenge through selective text embedding modification, enabling explicit semantic control over character identity without sacrificing prompt alignment. Furthermore, based on our analysis of padding embeddings in FLUX, we propose a semantic control strategy that repurposes padding embeddings as semantic containers. Additionally, we introduce an adaptive feature-sharing strategy that automatically evaluates textual ambiguity and applies constraints only to the ambiguous identity prompt. Finally, we propose a unified evaluation protocol, the Consistency Quality Score (CQS), which integrates identity preservation and per-image text alignment into a single comprehensive metric, explicitly capturing performance imbalances between the two metrics. Our framework achieves state-of-the-art performance, effectively overcoming prior trade-offs. Project page: <https://minjung-s.github.io/asemconsist>

## 1. Introduction

Recent text-to-image (T2I) generative models enable high-quality visuals closely aligned with textual prompts. Building on this success, *identity-consistent generation*, the task of creating coherent image sequences with consistent character identities, is increasingly important for narrative-driven content, animation, and interactive storytelling [8, 22, 29, 31]. Models such as NanoBanana<sup>1</sup> highlight this growing demand.

A key challenge in identity-consistent generation is the trade-off between identity preservation and per-image prompt alignment. For example, ConsiStory [29] and StoryDiffusion [35] maintain consistent identities but often produce fixed poses or unrealistic shapes. Meanwhile, 1Prompt1Story [22] improves identity consistency but struggles with prompt alignment. These methods rely on U-Net-based architectures [23], limiting their performance on complex textual descriptions. Similarly, CharaConsist [31] struggles when identity descriptions under-specified (e.g., “a man”).

How can we resolve this trade-off without strict architectural constraints? Inspired by prior works manipulating embeddings to control semantics [1, 11], we hypothesize that identity semantics influence all text embeddings. Thus, we directly modify text embeddings, which condition the entire generation process. Specifically, we propose a selective em-

\*Joint first authors; equal contribution.

†Corresponding author

<sup>1</sup>We exclude NanoBanana, as it is closed-source and requires paid credits for extensive use.

bedding modification that (i) amplifies components aligned with both shared identity and per-image descriptions, and (ii) suppresses identity-irrelevant components. Unlike prior methods [22], which handle identity and prompt alignment separately, our unified embedding approach simultaneously addresses both.

Additionally, we repurpose padding embeddings from <pad> tokens in FLUX [4] as semantic containers. Unlike padding embeddings in CLIP-conditioned U-Net models that inherently contain rich semantics [17], we observe that T5 padding embeddings [24], used by FLUX, predominantly encode prompt-irrelevant “dummy” directions. To address this, we inject meaningful semantics derived from per-image prompts into padding embeddings while selectively removing irrelevant components. By directly leveraging conditioning embeddings, our method provides a stronger semantic channel than joint attention-based methods [30]. Additionally, we empirically analyze the adverse effect of dummy semantics, motivating our decision to limit the length of active padding embeddings.

We further identify a critical limitation of previous identity preservation methods relying on uniform image feature sharing [29, 31, 35]. Typically, detailed appearance descriptions (e.g., “a zebra”) inherently ensure identity consistency without additional constraints, whereas ambiguous descriptions (e.g., “a man”) require explicit feature sharing. However, existing methods uniformly apply identity preservation regardless of textual ambiguity, causing inconsistent performance. To address this, we propose an adaptive feature-sharing mechanism that automatically evaluates textual ambiguity and selectively applies feature sharing only when needed.

Finally, prior studies typically evaluate identity preservation and per-image prompt alignment separately, failing to capture their combined performance in a single metric. To remedy this, we introduce the *Consistency Quality Score (CQS)*, a unified metric that integrates both aspects and explicitly penalizes performance imbalances. Beyond identity-consistent generation, CQS offers a principled solution to evaluation challenges in tasks requiring balanced multi-objective assessments [9, 27].

Our main contributions can be summarized as follows:

- We propose a selective text-embedding modification method that simultaneously achieves identity consistency and per-image text alignment.
- We identify that FLUX padding embeddings are dominated by “dummy” semantics and propose repurposing them as semantic containers.
- We introduce an adaptive feature-sharing method that selectively applies constraints based on textual ambiguity.
- We present a unified evaluation protocol, the *Consistency Quality Score*, integrating identity preservation and per-image prompt alignment into a single balanced metric.

## 2. Related works

### 2.1. Identity-consistent image generation

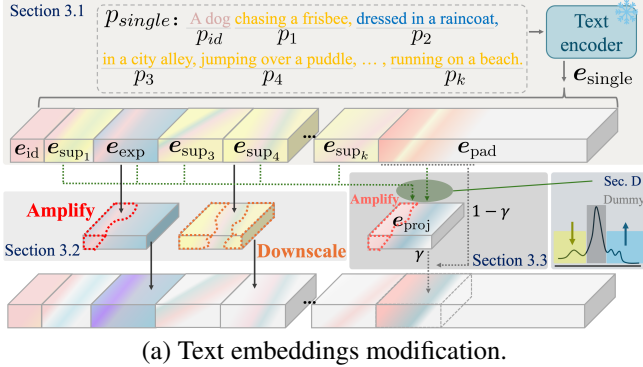
Identity-consistent generation seeks to maintain subject identity across images while staying faithful to each prompt. Recent works tackle compositional diversity [8] to hand-drawn story synthesis [34], all targeting both identity preservation and text alignment. A common strategy shares cross-image features via attention [29, 31, 35], but this can yield fixed poses and reduce alignment to per-image prompts. Other approaches train additional encoders or fine-tune the model [13, 16, 18, 20, 26, 28, 32, 33], but they often suffer from restricted domains or a trade-off between identity preservation and text alignment. Moreover, models that take reference images as input [16, 28, 32, 33] often highly depend on the given examples, resulting in limited diversity and poor generalization to appearance or pose variations. Alternatively, 1Prompt1Story [22] applies a fixed per-prompt schedule that uniformly increases or decreases the singular values of a shared text embedding, often entangling identity with prompt-specific attributes. In contrast, our method selectively adjusts the singular values of the text embeddings according to rules derived from their singular vectors, and further employs adaptive feature sharing to better preserve the consistency of a subject identity.

### 2.2. Metrics for consistent image generation

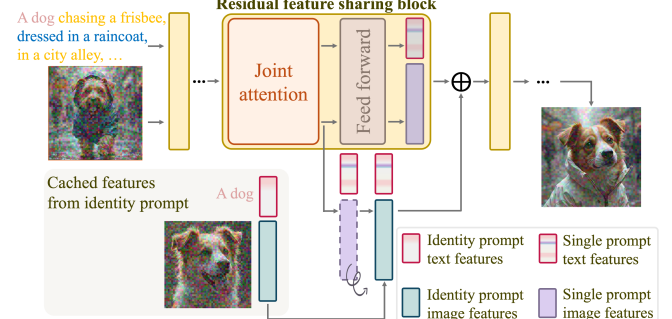
Identity preservation and per-image text alignment are main metrics to evaluate identity-consistent generation. Standard evaluation uses VQAScore [19] for text alignment by asking a VLM model whether the image matches the textual description, and DINO or DreamSim [6, 10] for identity preservation based on feature-similarity metrics. Evaluating the two scores separately does not yield a consistent ordering of models when text alignment and identity preservation are taken into account jointly. We propose a unified score that aggregates both criteria and penalizes their imbalance, yielding a single number that summarizes consistent-generation performance.

## 3. Methods

In this section, we first describe our problem setting (Sec. 3.1). Next, we introduce our text embedding modification strategy, which simultaneously ensures identity consistency and per-image prompt alignment (Sec. 3.2), and describe the use of padding embeddings as semantic containers (Sec. 3.3). Finally, we emphasize that the need for identity-specific constraints depends on the ambiguity of the identity prompt; thus, we propose an adaptive feature-sharing mechanism that automatically assesses identity ambiguity and selectively applies feature sharing only when needed (Sec. 3.4).



(a) Text embeddings modification.



(b) Adaptive feature sharing in Sec. 3.4.

Figure 2. Overall overview of our method. (a) illustrates the problem setting and text embedding modification, while (b) shows our adaptive feature sharing strategy that leverages image features to resolve ambiguity.

### 3.1. Problem setting

Our goal is to generate a sequence of coherent images that share a consistent character identity. Formally, an identity-consistent generation framework takes as input an identity prompt  $p_{\text{id}}$ , which describes the identity to be consistently preserved, along with multiple per-image prompts  $\{p_i\}_{i=1}^k$  specifying individual scene descriptions.

Modifying embeddings within a single combined prompt is an effective strategy for identity preservation [22]. Following this setting, we construct a single prompt by concatenating the identity prompt and all per-image prompts:

$$p_{\text{single}} = [p_{\text{id}}, p_1, \dots, p_k].$$

Given the combined prompt  $p_{\text{single}}$  of length  $L_{\text{single}}$ , the text encoder  $E(\cdot)$  produces a single embedding:

$$e_{\text{single}} = [e_{\text{id}}, e_1, \dots, e_k] \in \mathbb{R}^{L_{\text{single}} \times d},$$

where  $d$  denotes the embedding dimension and  $e_* \in \mathbb{R}^{L_* \times d}$  correspond to  $p_*$ . Importantly, the prompts  $p_*$  influence all embeddings  $e_*$ <sup>2</sup>.

When generating an image corresponding to a specific prompt  $p_i$ , we denote this prompt as the *expression prompt*  $e_{\text{exp}}$  with its embedding  $e_{\text{exp}}$ . The remaining prompts  $\{p_j\}_{j \in \{1, \dots, k\} \setminus \{i\}}$ , which should not influence the current image, are termed *suppression prompts*, with corresponding embeddings denoted as  $e_{\text{sup}_j}$ .

As illustrated in Fig. 2a, to generate an image from the second per-image prompt (e.g., “dressed in a raincoat”), we form embeddings:

$$[e_{\text{id}}, e_{\text{sup}_1}, e_{\text{exp}}, e_{\text{sup}_3}, \dots, e_{\text{sup}_k}],$$

explicitly express the desired attributes (e.g., the dog and its raincoat) while suppressing irrelevant information from other prompts. The effectiveness of a single prompt in FLUX is discussed in the Sec. A.

<sup>2</sup>Although our notation  $e_*$  denotes a matrix consisting of token-wise embedding vectors, we treat it as an embedding for simplicity.

### 3.2. Selective Text Embedding Modification

Under the single-prompt setting, individual embeddings  $e_i$  within the combined embedding  $e_{\text{single}}$  exhibit entangled semantics across dimensions [7, 14, 25]. This entanglement hinders precise control of embedding components needed for identity consistency and text alignment. To address this, we propose a selective embedding modification approach (illustrated in Fig. 2a) that *amplifies semantic features shared by identity and expression prompts*, while *suppressing identity-irrelevant components*. Briefly, our method consists of three steps performed in both the expression and suppression stages: (1) constructing a reference embedding and deriving a reference vector, which captures the semantic directions we intend to amplify or suppress and serves as an anchor for component selection; (2) selecting embedding components based on their similarity to the reference vector; (3) rescaling the selected components and reconstructing the modified embeddings.

**Selective expression.** First, we construct a reference embedding by concatenating identity and expression embeddings:

$$e_{\text{ref-exp}} = [e_{\text{id}}, e_{\text{exp}}].$$

We then apply Singular Value Decomposition (SVD) separately to  $e_{\text{exp}}$  and  $e_{\text{ref-exp}}$ , obtaining singular vectors and singular values  $\{\mathbf{v}_i, \sigma_i\}_{i=1}^{L_{\text{exp}}}$  for  $e_{\text{exp}}$  and  $\{\mathbf{v}_i, \sigma_i\}_{i=1}^{L_{\text{ref-exp}}}$  for  $e_{\text{ref-exp}}$ , where  $L_{\text{ref-exp}} = L_{\text{id}} + L_{\text{exp}}$ . We define a reference vector:

$$\mathbf{v}_{\text{ref-exp}} = \sum_{i=1}^{L_{\text{ref-exp}}} \sigma_i \mathbf{v}_i, \quad (1)$$

with orientations aligned to the weighted mean of  $e_{\text{exp}}$  to resolve sign ambiguity, following standard PCA/SVD conventions [5].

Secondly, we compute cosine similarity between singular vectors  $\mathbf{v}_i$  and  $\mathbf{v}_{\text{ref-exp}}$ , defining an adaptive threshold:

$$\zeta_{\text{exp}} = \frac{1}{L_{\text{exp}}} \sum_{i=1}^{L_{\text{exp}}} \cos(\mathbf{v}_i, \mathbf{v}_{\text{ref-exp}}).$$

Components with similarity above  $\zeta_{\text{exp}}$  are marked as expression-relevant and will be amplified.

Finally, we amplify the corresponding singular values using

$$\sigma_i \leftarrow U_{\text{exp}}(\sigma_i), \quad \text{if } \cos(\mathbf{v}_i, \mathbf{v}_{\text{ref-exp}}) > \zeta_{\text{exp}}, \quad (2)$$

with the amplification function defined as  $U_{\text{exp}}(\sigma) = \beta e^{\alpha \sigma} \sigma$ . We then reconstruct the amplified text embeddings using the updated singular values. This text feature modification also applies within transformer blocks before Rotary Positional Embedding (RoPE) (see Sec. B).

**Selective suppression.** We use the identity embedding  $e_{\text{id}}$  as the reference embedding  $e_{\text{ref-sup}}$  to select identity-irrelevant components in suppression embeddings. Similar to the selective expression step, we apply SVD separately to the suppression embedding  $e_{\text{sup}}$  and the reference embedding  $e_{\text{ref-sup}}$ , obtaining singular vectors and singular values  $\{\mathbf{v}_j, \sigma_j\}_{j=1}^{L_{\text{sup}}}$  and  $\{\mathbf{v}_j^{\text{ref-sup}}, \sigma_j^{\text{ref-sup}}\}_{j=1}^{L_{\text{id}}}$ , respectively. We define the reference vector  $\mathbf{v}_{\text{ref-sup}}$  from  $e_{\text{ref-sup}}$  in the same way as in Eq. (1).

Secondly, we compute cosine similarity between each singular vector  $\mathbf{v}_j$  from  $e_{\text{sup}}$  and the reference vector  $\mathbf{v}_{\text{ref-sup}}$ , and define the adaptive threshold

$$\zeta_{\text{sup}} = \frac{1}{L_{\text{sup}}} \sum_{j=1}^{L_{\text{sup}}} \cos(\mathbf{v}_j, \mathbf{v}_{\text{ref-sup}}).$$

Components with similarity below  $\zeta_{\text{sup}}$  are regarded as identity-irrelevant and will be suppressed.

Finally, we downscale the singular values of the selected components using

$$\sigma_j \leftarrow D_{\text{sup}}(\sigma_j), \quad \text{if } \cos(\mathbf{v}_j, \mathbf{v}_{\text{ref-sup}}) < \zeta_{\text{sup}}, \quad (3)$$

where the downscaling function is defined as  $D_{\text{sup}}(\sigma) = \beta' e^{-\alpha' \sigma} \sigma$ . We apply selective suppression iteratively to all  $e_{\text{sup}_j}$  and then reconstruct the suppressed text embeddings using the updated singular values.

### 3.3. Semantic projection on padding embeddings

We observe that padding embeddings in FLUX contain only limited prompt-related semantics and are largely dominated by prompt-irrelevant “dummy” directions, unlike the semantically rich padding embeddings found in U-Net-based models [17]. Motivated by this, we repurpose T5 padding

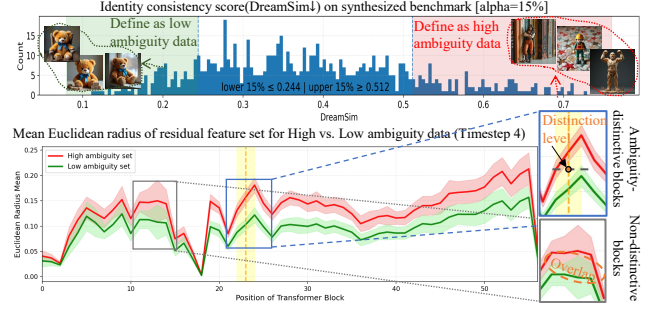


Figure 3. Cosine similarity distributions of residual features from prompt sets  $\{p_{\text{id}}, p_1\}, \dots, \{p_{\text{id}}, p_k\}$  at different transformer blocks. At ambiguity-distinctive blocks (yellow box), high-ambiguity (red; samples with high DreamSim scores) and low-ambiguity sets (green; samples with low DreamSim scores) are clearly separable. At non-distinctive blocks, distributions overlap, hindering ambiguity discrimination.

embeddings [24] as auxiliary semantic containers. We inject per-image prompt-aligned semantics into the padding embedding while removing suppression semantics associated with the dummy direction. The resulting refined padding embeddings are then reused in our selective expression mechanism to reinforce expression-specific semantics in the padding space. The observations motivating this design are discussed in Secs. D and 4.2.

We achieve this adaptive semantic projection in two steps. First, we incorporate semantics aligned with the expression embedding:

$$\mathbf{e}_{\text{pad}} \leftarrow (1 - \gamma) \mathbf{e}_{\text{pad}} + \gamma \mathbf{e}_{\text{proj-exp}}. \quad (4)$$

Then, we remove redundancy aligned with the suppression embedding:

$$\mathbf{e}_{\text{pad}} \leftarrow \mathbf{e}_{\text{pad}} - \gamma \mathbf{e}_{\text{proj-sup}}. \quad (5)$$

Here,  $\mathbf{e}_{\text{proj-exp}}$  and  $\mathbf{e}_{\text{proj-sup}}$  are the projections of  $\mathbf{e}_{\text{pad}}$  onto the expression and suppression embeddings, respectively, computed as follows:

$$\mathbf{e}_{\text{proj}} = (P_i^{\top} \mathbf{e}_{\text{pad}}^{\top})^{\top}, \quad (6)$$

where  $P_i = \mathbf{e}_i^{\top} (\mathbf{e}_i \mathbf{e}_i^{\top})^{\dagger} \mathbf{e}_i$ ,

with  $(\cdot)^{\dagger}$  denoting the pseudo-inverse. Specifically,  $\mathbf{e}_i$  is set to  $\mathbf{e}_{\text{exp}}$  for  $\mathbf{e}_{\text{proj-exp}}$ , and to  $\mathbf{e}_{\text{sup}}$  for  $\mathbf{e}_{\text{proj-sup}}$ . This semantic projection allows padding embeddings to serve explicitly as controlled semantic containers, significantly enhancing per-image prompt alignment.

Additionally, during selective expression, we use only the first  $L_{\text{exp}}$  padding embeddings, denoted as  $\mathbf{e}_{\text{pad-sub}} \in \mathbb{R}^{L_{\text{exp}} \times d}$ , concatenated with  $\mathbf{e}_{\text{exp}}$ . This subset choice prevents irrelevant “dummy” semantics from interfering with expression-related component amplification.

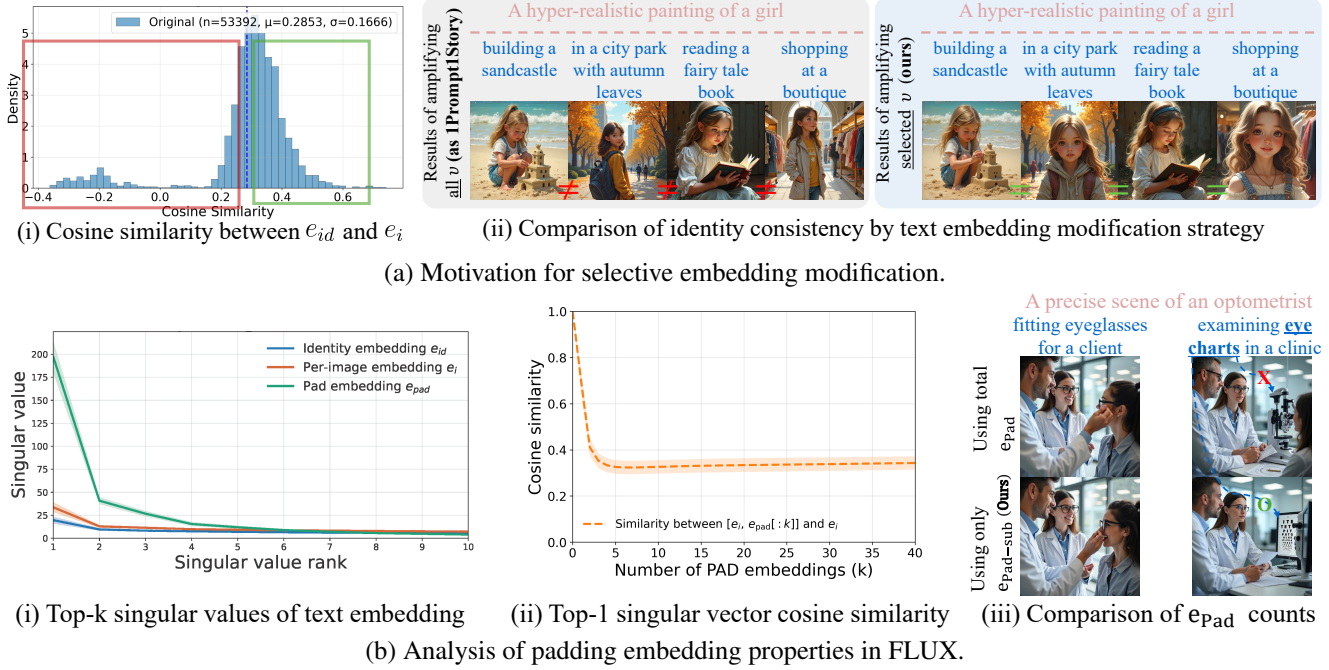


Figure 4. Analysis and validation of our text embedding modification. We use about 100 samples from the benchmark for this analysis. In the generated sample figure, the identity prompts are shown in pink, and per-image prompts are shown in blue.

### 3.4. Adaptive feature sharing

As discussed, detailed identity descriptions inherently preserve identity consistency through embedding modifications alone. However, ambiguous descriptions require additional mechanisms. Thus, we propose *Adaptive Feature Sharing*, which automatically assesses identity ambiguity and selectively applies feature sharing.

To determine the ambiguity level of an identity prompt, we analyze prompt sets  $\{p_{id}, p_1\}, \dots, \{p_{id}, p_k\}$  to identify transformer blocks and denoising timesteps where feature cohesion clearly distinguishes high- from low-ambiguity cases. As shown in Fig. 3, transformer blocks 23 at denoising timestep 4 exhibit the most pronounced separability. Detailed threshold selection criteria are provided in Sec. C.

When the identity prompt  $p_{id}$  is classified as highly ambiguous, we apply residual feature sharing instead of traditional attention-based methods [29, 35] to avoid positional biases. As shown in previous studies [15], residual features implicitly encode identity-related information without interfering with per-image alignment. Specifically, we first cache residual features conditioned solely on  $p_{id}$ , then replace corresponding residual features during subsequent generation steps, as depicted in Fig. 2b. This adaptive strategy reinforces identity consistency without performance degradation due to variations in character descriptions.

## 4. Analysis

### 4.1. Reason for selective embedding modification

This section explains the motivation behind our selective embedding modification (Sec. 3.2). As shown in Fig. 4a-(i), per-image embeddings ( $e_i$ ) contain both intended semantics and entangled identity attributes. Components positively aligned with the identity embedding ( $e_{id}$ , green region in Fig. 4a)-(i) represent semantics jointly relevant to the per-image description and shared identity. Our selective expression step amplifies these components, improving both expression fidelity and identity coherence.

However, embeddings also contain negatively correlated components (red region in Fig. 4a-(i)), rather than being simply orthogonal. Previous methods [22], which uniformly scale all singular values of  $e_i$ , fail to account for such negative alignments, causing semantic drift and reduced identity consistency. As illustrated in Fig. 4a-(ii) (gray box), uniform scaling compromises identity consistency. Conversely, our selective method amplifies only consistently aligned components across embeddings, preserving identity coherence and per-image fidelity (blue box in Fig. 4a-(ii)).

Similarly, in selective suppression, our method down-scales only components unrelated to identity. In contrast, previous methods [22] uniformly downscale all compo-

nents of the suppression embedding, which also suppresses identity-related semantics and consequently disrupts identity consistency. Overall, our selective strategies maintain coherent identity representations without sacrificing per-image prompt alignment.

## 4.2. Dominant information in padding embeddings

We further demonstrate that padding embeddings contain a dominant semantic direction largely unrelated to the intended prompt semantics. This finding directly motivates our decision to utilize only a subset of padding embeddings in our selective text embedding modification.

As illustrated by the green line in Fig. 4b-(i), the singular values of the padding embeddings  $e_{\text{pad}}$  are strongly dominated by a single large component, while the remaining values are significantly smaller and nearly uniform. This indicates that padding embeddings collapse onto one dominant semantic direction. In contrast, the identity embedding  $e_{\text{id}}$  and per-image embeddings  $e_i$  exhibit a more gradual decay of singular values, reflecting richer and more diverse semantics.

This dominant direction in  $e_{\text{pad}}$  primarily corresponds to irrelevant "dummy" semantics rather than meaningful, prompt-related information. To verify this, we measure the similarity between a per-image embedding  $e_i$  and its extended form obtained by concatenating the first  $n$  tokens of  $e_{\text{pad}}$ , denoted as  $[e_i, e_{\text{pad}}[:n]]$ . As shown in the green line of Fig. 4b-(ii), similarity with the original  $e_i$  sharply decreases as  $n$  increases, whereas similarity with  $e_{\text{pad}}$  steadily rises. This demonstrates that additional padding tokens introduce semantics dominated by irrelevant dummy information rather than intended prompt semantics. Consequently, using a large number of padding embeddings in selective text embedding modification can degrade per-image prompt alignment, as dominant "dummy" semantics adversely affect the threshold for semantic selection, as illustrated in the upper sample of Fig. 4b-(iii). Conversely, restricting padding embeddings to a smaller subset, as in our approach, significantly improves prompt alignment.

These findings justify our design choice to use only a limited subset of padding embeddings. Due to the lack of rich semantic information in T5 padding embeddings and their dominance by a single "dummy" semantic direction, we explicitly inject per-image prompt semantics into the padding embeddings and restrict their use to a controlled sub-space.

## 5. Experiments

### 5.1. Balanced evaluation: Consistency Quality Score (CQS)

Existing protocols evaluate identity consistency and per-image prompt alignment separately using metrics such as

VQAScore [19] and DreamSim. This separation makes it hard to form a balanced ranking of a model's overall ability. To address this, we introduce the Consistency Quality Score,  $CQS_{\text{har}}$ , which computes the harmonic mean of the alignment and identity scores to provide a single, interpretable, and balance-aware metric.

Given a combined prompt set  $[p_{\text{id}}, p_1, \dots, p_k]$  and corresponding generated images  $X = \{x_1, \dots, x_k\}$ , each image  $x_i$  is generated by emphasizing its corresponding per-image prompt  $p_i$  and suppressing other prompts. For each image  $x_i$ , we define two distinct alignment scores:

$$t_i = VQA(x_i, [p_{\text{id}}, p_i]) \quad \text{and} \quad a_i = VQA(x_i, p_i), \quad (7)$$

where  $t_i$  measures alignment with the combined identity and per-image prompts, and  $a_i$  measures alignment solely with the per-image prompt. To quantify identity consistency across the generated image set  $X$ , we define the identity similarity score  $d_i$  using DreamSim as follows:

$$d_i = \frac{1}{k-1} \sum_{\substack{j=1 \\ j \neq i}}^k D(x_i, x_j). \quad (8)$$

DreamSim scores are transformed using  $(1 - \cdot)$  and scaled to match the range of VQA scores via min–max scaling, ensuring equal weighting of the two metrics in the harmonic mean.

To penalize cases where per-image alignment underperforms relative to the combined alignment, we define the alignment gap  $\Delta_i = a_i - t_i$  and compute dataset-level mean positive and negative gaps:

$$\bar{\Delta}_+ = \mathbb{E}[\Delta_i \mid \Delta_i > 0], \quad \bar{\Delta}_- = \mathbb{E}[\Delta_i \mid \Delta_i < 0]. \quad (9)$$

For each sample, we define penalty and reward terms:

$$\begin{aligned} \delta_i^- &= (1 - \lambda) \bar{\Delta}_- + \lambda \max(-\Delta_i, 0), \\ \delta_i^+ &= (1 - \lambda) \bar{\Delta}_+ + \lambda \max(\Delta_i, 0), \end{aligned} \quad (10)$$

where  $\lambda \in [0, 1]$  balances dataset-level and instance-level adjustments. The adjusted identity score is then:

$$d_i^* = d_i - \mu \mathbf{1}[\Delta_i < 0] \delta_i^- + \tau \mathbf{1}[\Delta_i > 0] \delta_i^+, \quad (11)$$

with  $\mu, \tau \geq 0$  controlling the strength of penalties and rewards.<sup>3</sup>

The final per-sample score is a harmonic mean:

$$h_i = \frac{2 t_i d_i^*}{t_i + d_i^* + \varepsilon}, \quad (12)$$

where  $\varepsilon > 0$  ensures numerical stability. The overall CQS score is the mean of all per-sample scores:

$$CQS_{\text{har}} = \frac{1}{N} \sum_{i=1}^N h_i. \quad (13)$$

<sup>3</sup>We set  $\mu, \tau = 0.5$  for equal treatment, and  $\lambda = 1$  by default.

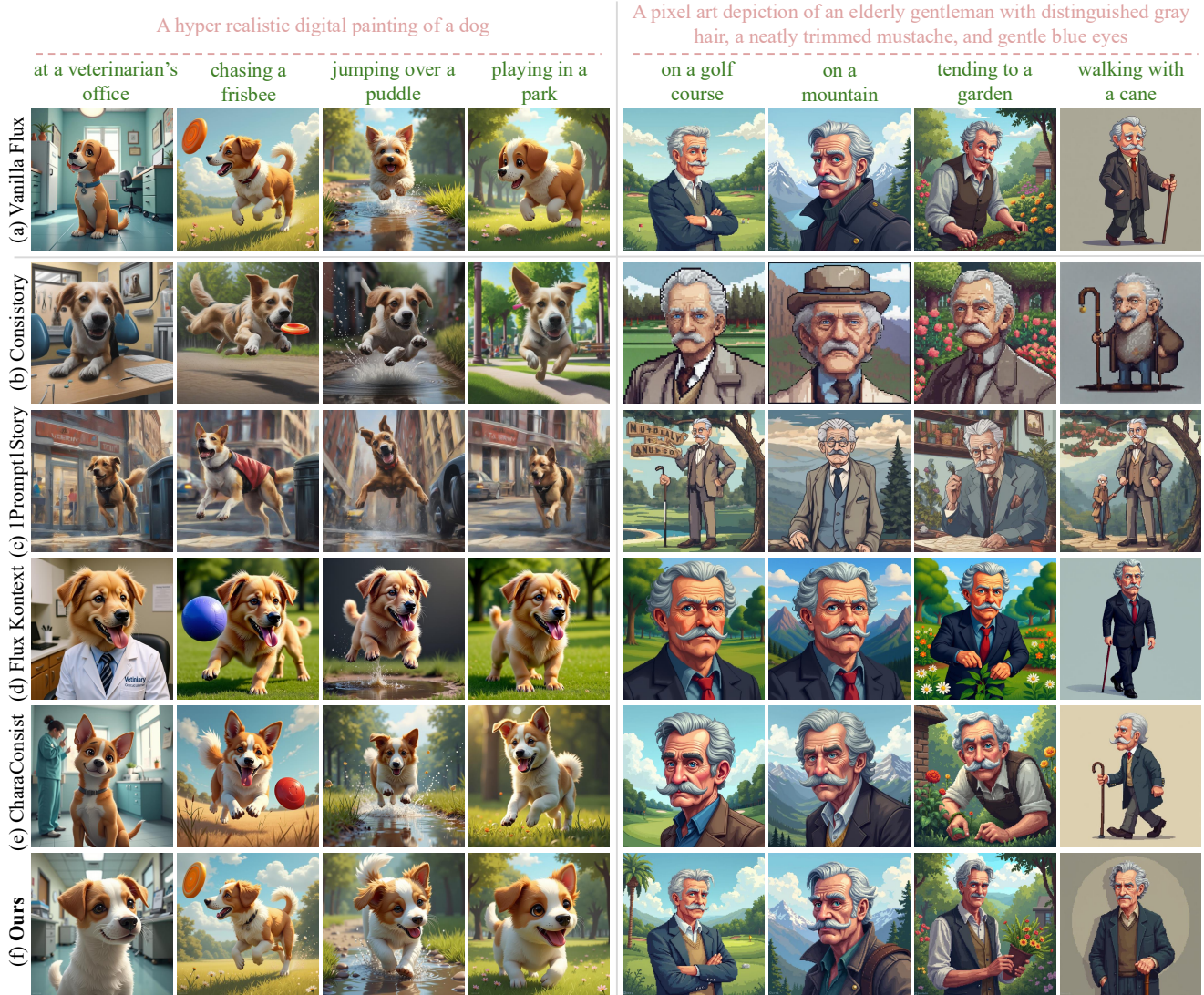


Figure 5. Qualitative comparison. The identity prompt (pink text) describes the character identity shared across the image sequence, while per-image prompts (green) specify attributes unique to each image.

By explicitly addressing performance imbalances between identity consistency and prompt alignment, the proposed  $CQS_{har}$  metric provides a balanced, comprehensive, and interpretable evaluation for identity-consistent generation methods.

## 5.2. Experimental setup

To comprehensively evaluate our approach and identify inherent limitations of backbone-only models, we include comparisons with the FLUX baseline [4], which generates images by directly conditioning on concatenated identity and per-image prompts  $\{p_{id}, p_i\}_{i=1}^k$ . We also compare with recent identity-consistent generation methods, including U-Net-based methods (ConsiStory [29], 1Prompt1Story [22])

	$CQS_{har} \uparrow$	Per-image text alignment $\uparrow$	Identity consistency $\downarrow$
FLUX	0.488	0.631	0.429
Consistency	0.426	0.517	0.398
1Prompt1Story	0.258	0.300	0.378
FLUX-kontext	0.539	0.556	0.200
CharaConsist	0.443	0.590	0.468
<b>ASemConsist (Ours)</b>	<b>0.553</b>	<b>0.627</b>	<b>0.302</b>

Table 1. Quantitative results. We highlight the best score in light red and the second-best in yellow. Ours achieves state-of-the-art performance on the  $CQS_{har}$ , balancing per-image alignment and identity consistency.

using the SDXL backbone [23], and DiT-based methods (CharaConsist [31]) built on FLUX. Additionally, we evaluate against FLUX-Kontext [16], which generates images conditioned on a reference image and text prompts. For FLUX-Kontext, we first generate a reference image from the identity prompt  $p_{id}$  using FLUX, and subsequently produce images conditioned on this reference image along with individual per-image prompts  $p_i$ . We report results using our proposed balanced evaluation protocol  $CQS_{har}$ , as well as average prompt alignment and pairwise identity consistency scores. Further details on the text benchmark for evaluation are provided in the Sec. E.

### 5.3. Comparison

As our method is training-free, we compare it with other training-free approaches, and the results are presented in Tab. 1. Our method achieves state-of-the-art performance on the proposed  $CQS_{har}$ , indicating that it better maintains the balance between identity consistency and per-image text alignment.

1Prompt1Story attains high identity consistency but exhibits substantially worse per-image text alignment due to its non-adaptive method, leading to a low  $CQS_{har}$ . Image feature sharing methods, such as ConsiStory and CharaConsist, struggle to maintain identity consistency, especially under highly ambiguous descriptions (e.g., “a dog”). Whenever a vanilla pretrained T2I model, such as FLUX, fails to preserve identity under weak or underspecified prompts, feature-sharing methods inevitably inherit the same limitation. Although recent image-conditioned methods like FLUX Kontext provide strong identity preservation, they are heavily constrained by the pose and scale of the conditioned image, often generating images that deviate from the text prompts. Qualitative comparisons in Fig. 5 highlight these failure modes.

In contrast, our method combines selective text embedding modification with an adaptive feature sharing strategy, enabling explicit control over the trade-off between per-image prompt alignment and identity consistency, and remaining robust even under ambiguous descriptions. Additional qualitative examples are provided in the supplementary material.

### 5.4. Ablation Study

We evaluate the effectiveness of each proposed component and its combined impact on identity consistency and prompt alignment. As shown in Tab. 1, our complete method (e), combining selective text embedding modification (STM), semantic projection on padding embeddings (PAD), and adaptive feature sharing (AFS), achieves the highest  $CQS_{har}$  score, demonstrating balanced improvements.

Comparing case (b) with FLUX baseline (a), STM sig-

	$CQS_{har} \uparrow$	Per-image text alignment $\uparrow$	Identity consistency $\downarrow$
(a) FLUX	0.488	0.631	0.429
(b) FLUX + STM	0.541	0.625	0.324
(c) FLUX + STM&PAD	0.543	0.628	0.326
(d) FLUX + AFS	0.500	0.622	0.396
(e) Ours	0.553	0.627	0.302

Table 2. Performance comparison and ablation study from the FLUX baseline to our proposed method, adding selective text embedding modification (STM), semantic projection on padding embeddings (PAD), and adaptive feature sharing (AFS). The best scores are highlighted in light red and second-best in yellow.

nificantly enhances identity consistency, showing that identity semantics are globally encoded even without directly modifying identity embeddings. Furthermore, comparing cases (b) and (c) confirms that our PAD strategy notably improves prompt alignment, validating padding embeddings as effective semantic containers.

Comparing cases (d) and (e) reveals that our adaptive feature sharing is most effective when combined with STM and PAD. This is because residual features encode only coarse identity-related information implicitly [15]. However, by ensuring identity consistency through our modified text embeddings and semantic-enriched padding embeddings, residual feature sharing can effectively reinforce identity without over-encoding unwanted shape or pose information from cached image features that would otherwise compromise per-image prompt fidelity.

Qualitative results and additional ablation studies are provided in Sec. G.

## 6. Conclusion

In this paper, we addressed the trade-off between identity consistency and per-image text alignment. We showed that selective text-embedding modification can control globally encoded identity semantics without degrading text-alignment quality. We also identified that T5 padding embeddings in FLUX mainly encode prompt-irrelevant “dummy” semantics and demonstrated that reusing them as semantic containers improves alignment. In addition, we introduced an adaptive residual feature-sharing mechanism that activates only under high textual ambiguity. Finally, we presented the Consistency Quality Score (CQS), a unified metric that evaluates identity consistency and per-image alignment.

These findings highlight the importance of precise semantic control in text embeddings and adaptive constraints determined by identity-prompt ambiguity. Moreover, our unified evaluation metric can generalize to other tasks that require joint assessment of multiple criteria, offering practical value for the research community.

## References

[1] Ruichuan An, Sihan Yang, Renrui Zhang, Zijun Shen, Ming Lu, Gaole Dai, Hao Liang, Ziyu Guo, Shilin Yan, Yulin Luo, et al. Unictokens: Boosting personalized understanding and generation via unified concept tokens. *arXiv preprint arXiv:2505.14671*, 2025. 1

[2] Omri Avrahami, Or Patashnik, Ohad Fried, Egor Nemchinov, Kfir Aberman, Dani Lischinski, and Daniel Cohen-Or. Stable flow: Vital layers for training-free image editing. In *Proceedings of the Computer Vision and Pattern Recognition Conference*, pages 7877–7888, 2025. 1

[3] Shuai Bai, Keqin Chen, Xuejing Liu, Jialin Wang, Wenbin Ge, Sibo Song, Kai Dang, Peng Wang, Shijie Wang, Jun Tang, et al. Qwen2. 5-vl technical report. *arXiv preprint arXiv:2502.13923*, 2025. 3

[4] Black Forest Labs. Flux. <https://github.com/black-forest-labs/flux>, 2024. 2, 7, 3

[5] Rasmus Bro, Evrim Acar, and Tamara G Kolda. Resolving the sign ambiguity in the singular value decomposition. *Journal of Chemometrics: A Journal of the Chemometrics Society*, 22(2):135–140, 2008. 3

[6] Mathilde Caron, Hugo Touvron, Ishan Misra, Hervé Jégou, Julien Mairal, Piotr Bojanowski, and Armand Joulin. Emerging properties in self-supervised vision transformers. In *Proceedings of the IEEE/CVF international conference on computer vision*, pages 9650–9660, 2021. 2

[7] Hila Chefer, Yuval Alaluf, Yael Vinker, Lior Wolf, and Daniel Cohen-Or. Attend-and-excite: Attention-based semantic guidance for text-to-image diffusion models. *ACM transactions on Graphics (TOG)*, 42(4):1–10, 2023. 3

[8] David Dinkevich, Matan Levy, Omri Avrahami, Dvir Samuel, and Dani Lischinski. Story2board: A training-free approach for expressive storyboard generation. *arXiv preprint arXiv:2508.09983*, 2025. 1, 2

[9] Tao Feng, Yifan Xie, Xun Guan, Jiyuan Song, Zhou Liu, Fei Ma, and Fei Yu. Unisync: A unified framework for audio-visual synchronization. *arXiv preprint arXiv:2503.16357*, 2025. 2

[10] Stephanie Fu, Netanel Tamir, Shobhita Sundaram, Lucy Chai, Richard Zhang, Tali Dekel, and Phillip Isola. Dreamsim: Learning new dimensions of human visual similarity using synthetic data. *arXiv preprint arXiv:2306.09344*, 2023. 2, 3

[11] Rinon Gal, Yuval Alaluf, Yuval Atzmon, Or Patashnik, Amit H Bermano, Gal Chechik, and Daniel Cohen-Or. An image is worth one word: Personalizing text-to-image generation using textual inversion. *arXiv preprint arXiv:2208.01618*, 2022. 1

[12] Jun Gao, Di He, Xu Tan, Tao Qin, Liwei Wang, and Tie-Yan Liu. Representation degeneration problem in training natural language generation models. *arXiv preprint arXiv:1907.12009*, 2019. 3

[13] Zinan Guo, Yanze Wu, Chen Zhuowei, Peng Zhang, Qian He, et al. Pulid: Pure and lightning id customization via contrastive alignment. *Advances in neural information processing systems*, 37:36777–36804, 2024. 2

[14] Jeeyung Kim, Erfan Esmaeili, and Qiang Qiu. Text embedding is not all you need: Attention control for text-to-image semantic alignment with text self-attention maps. In *Proceedings of the Computer Vision and Pattern Recognition Conference*, pages 8031–8040, 2025. 3

[15] Jimyeong Kim, Jungwon Park, Yeji Song, Nojun Kwak, and Wonjong Rhee. Reflex: Text-guided editing of real images in rectified flow via mid-step feature extraction and attention adaptation. *arXiv preprint arXiv:2507.01496*, 2025. 5, 8

[16] Black Forest Labs, Stephen Batifol, Andreas Blattmann, Frederic Boesel, Saksham Consul, Cyril Diagne, Tim Dockhorn, Jack English, Zion English, Patrick Esser, et al. Flux. 1 kontext: Flow matching for in-context image generation and editing in latent space. *arXiv preprint arXiv:2506.15742*, 2025. 2, 8, 3, 5

[17] Senmao Li, Joost van de Weijer, Taihang Hu, Fahad Shahbaz Khan, Qibin Hou, Yaxing Wang, and Jian Yang. Get what you want, not what you don't: Image content suppression for text-to-image diffusion models. *arXiv preprint arXiv:2402.05375*, 2024. 2, 4

[18] Zhen Li, Mingdeng Cao, Xintao Wang, Zhongang Qi, Ming-Ming Cheng, and Ying Shan. Photomaker: Customizing realistic human photos via stacked id embedding. In *Proceedings of the IEEE/CVF conference on computer vision and pattern recognition*, pages 8640–8650, 2024. 2

[19] Zhiqiu Lin, Deepak Pathak, Baiqi Li, Jiayao Li, Xide Xia, Graham Neubig, Pengchuan Zhang, and Deva Ramanan. Evaluating text-to-visual generation with image-to-text generation. In *European Conference on Computer Vision*, pages 366–384. Springer, 2024. 2, 6, 3

[20] Chang Liu, Haoning Wu, Yujie Zhong, Xiaoyun Zhang, Yanfeng Wang, and Weidi Xie. Intelligent grimm-open-ended visual storytelling via latent diffusion models. In *Proceedings of the IEEE/CVF Conference on Computer Vision and Pattern Recognition*, pages 6190–6200, 2024. 2

[21] Luping Liu, Chao Du, Tianyu Pang, Zehan Wang, Chongxuan Li, and Dong Xu. Improving long-text alignment for text-to-image diffusion models. *arXiv preprint arXiv:2410.11817*, 2024. 3

[22] Tao Liu, Kai Wang, Senmao Li, Joost van de Weijer, Fahad Shahbaz Khan, Shiqi Yang, Yaxing Wang, Jian Yang, and Ming-Ming Cheng. One-prompt-one-story: Free-lunch consistent text-to-image generation using a single prompt. *arXiv preprint arXiv:2501.13554*, 2025. 1, 2, 3, 5, 7

[23] Dustin Podell, Zion English, Kyle Lacey, Andreas Blattmann, Tim Dockhorn, Jonas Müller, Joe Penna, and Robin Rombach. Sdxl: Improving latent diffusion models for high-resolution image synthesis. *arXiv preprint arXiv:2307.01952*, 2023. 1, 8

[24] Colin Raffel, Noam Shazeer, Adam Roberts, Katherine Lee, Sharan Narang, Michael Matena, Yanqi Zhou, Wei Li, and Peter J Liu. Exploring the limits of transfer learning with a unified text-to-text transformer. *Journal of machine learning research*, 21(140):1–67, 2020. 2, 4

[25] Royi Rassin, Eran Hirsch, Daniel Glickman, Shauli Ravfogel, Yoav Goldberg, and Gal Chechik. Linguistic binding in diffusion models: Enhancing attribute correspondence

through attention map alignment. *Advances in Neural Information Processing Systems*, 36:3536–3559, 2023. 3

[26] Xiaoqian Shen and Mohamed Elhoseiny. Storygpt-v: Large language models as consistent story visualizers. In *Proceedings of the Computer Vision and Pattern Recognition Conference*, pages 13273–13283, 2025. 2

[27] Minjung Shin, Hyunin Cho, Sooyeon Go, Jin-Hwa Kim, and Youngjung Uh. Mvcustom: Multi-view customized diffusion via geometric latent rendering and completion. *arXiv preprint arXiv:2510.13702*, 2025. 2

[28] Zhenxiong Tan, Songhua Liu, Xingyi Yang, Qiaochu Xue, and Xinchao Wang. Ominicontrol: Minimal and universal control for diffusion transformer. *arXiv preprint arXiv:2411.15098*, 2024. 2

[29] Yoad Tewel, Omri Kaduri, Rinon Gal, Yoni Kasten, Lior Wolf, Gal Chechik, and Yuval Atzmon. Training-free consistent text-to-image generation. *ACM Transactions on Graphics (TOG)*, 43(4):1–18, 2024. 1, 2, 5, 7, 3

[30] Michael Toker, Ido Galil, Hadas Orgad, Rinon Gal, Yoad Tewel, Gal Chechik, and Yonatan Belinkov. Padding tone: A mechanistic analysis of padding tokens in t2i models. In *Proceedings of the 2025 Conference of the Nations of the Americas Chapter of the Association for Computational Linguistics: Human Language Technologies (Volume 1: Long Papers)*, pages 7618–7632, 2025. 2

[31] Mengyu Wang, Henghui Ding, Jianing Peng, Yao Zhao, Yunpeng Chen, and Yunchao Wei. Characonsist: Fine-grained consistent character generation. *arXiv preprint arXiv:2507.11533*, 2025. 1, 2, 8, 3

[32] Shitao Xiao, Yueze Wang, Junjie Zhou, Huaying Yuan, Xingrun Xing, Ruiran Yan, Chaofan Li, Shuting Wang, Tiejun Huang, and Zheng Liu. Omnigen: Unified image generation. In *Proceedings of the Computer Vision and Pattern Recognition Conference*, pages 13294–13304, 2025. 2

[33] Hu Ye, Jun Zhang, Sibo Liu, Xiao Han, and Wei Yang. Ipadapter: Text compatible image prompt adapter for text-to-image diffusion models. *arXiv preprint arXiv:2308.06721*, 2023. 2

[34] Jiayi Zheng and Xiaodong Cun. Fairygen: Storied cartoon video from a single child-drawn character. *arXiv preprint arXiv:2506.21272*, 2025. 2

[35] Yupeng Zhou, Daquan Zhou, Ming-Ming Cheng, Jiashi Feng, and Qibin Hou. Storydiffusion: Consistent self-attention for long-range image and video generation. *Advances in Neural Information Processing Systems*, 37:110315–110340, 2024. 1, 2, 5

# ASemConsist: Adaptive Semantic Feature Control for Training-Free Identity-Consistent Generation

## Supplementary Material

### A. Effectiveness of single prompt in FLUX baseline

In this section, we demonstrate the effectiveness of using a single combined prompt (identity prompt and all per-image prompts at once) compared to multiple separate prompts (identity prompt paired individually with each per-image prompt) in preserving identity consistency. Specifically, we analyze embedding cohesion in the T5 text encoder used by FLUX, analogous to the analysis conducted on SDXL’s CLIP embeddings in 1Prompt1Story [22].

As introduced in Sec. 3.1, we construct a single combined prompt by concatenating the identity and per-image prompts:

$$p_{\text{single}} = [p_{\text{id}}, p_1, \dots, p_k].$$

The T5 encoder  $E_{\text{T5}}(\cdot)$  generates the corresponding embeddings:

$$e_{\text{single}} = [e_{\text{id}}, e_1, \dots, e_k] \in \mathbb{R}^{L_{\text{single}} \times d},$$

where  $d$  denotes the embedding dimension and each  $e_* \in \mathbb{R}^{L_* \times d}$  corresponds to  $p_*$ . We extract identity and per-image embeddings by splitting this combined embedding based on token indices, yielding pairs  $[e_{\text{id}}, e_i]$ .

Conversely, in the multi-prompt setting, the identity prompt is concatenated individually with each per-image prompt, encoded separately as:

$$[e_{\text{id}}^{(i)}, e_{\text{multi}}^{(i)}] = E_{\text{T5}}([p_{\text{id}}, p_i]), \quad i \in \{1, \dots, k\}.$$

For evaluation, we use the official Consistency benchmark [29], consisting of 122 prompts and 727 identity/per-image pairs. We project the embeddings from both single- and multi-prompt settings onto a shared 2D space using t-SNE. We then calculate the average pairwise  $L_2$  distance between projected embeddings:

$$d_{\text{avg}}^{\text{t-SNE}} = \frac{1}{k(k-1)} \sum_{i \neq j} \|\mathbf{z}_i - \mathbf{z}_j\|_2,$$

where  $\mathbf{z}_i \in \mathbb{R}^2$  represents the t-SNE projection of embedding  $i$ .

As shown in Fig. A1a, embeddings from the single-prompt setting form significantly tighter clusters than those from the multi-prompt setting. Fig. A1b quantitatively confirms that single-prompt embeddings consistently have smaller average  $L_2$  distances, indicating stronger semantic cohesion.

This result implies that the single-prompt setting effectively encourages the T5 encoder to maintain consistent identity semantics across diverse scenes, whereas the multi-prompt approach encodes identities independently per image, resulting in more dispersed representations. Consequently, our single-prompt formulation promotes stronger semantic coherence and improved identity consistency in the embedding space.

### B. Implementation detail

#### B.1. Backbone and GPU setting

We implement our method on top of the FLUX-dev backbone and conduct all experiments on a single NVIDIA RTX A6000 GPU.

#### B.2. Adaptive feature sharing

Adaptive feature sharing (AFS) is applied to the residual stream at transformer blocks [0, 1, 2, 17, 18] during the early denoising steps  $t \in [1, 6]$ .

#### B.3. Selective text embedding modification

Selective text embedding modification (STM) is applied only to the expression prompt at blocks [25, 28, 53, 54, 56] for steps  $t \in [7, 11]$ , operating at the *before head reshape* level of the DiT attention module. The overall generation uses a 28-step denoising schedule, with STM scaling parameters

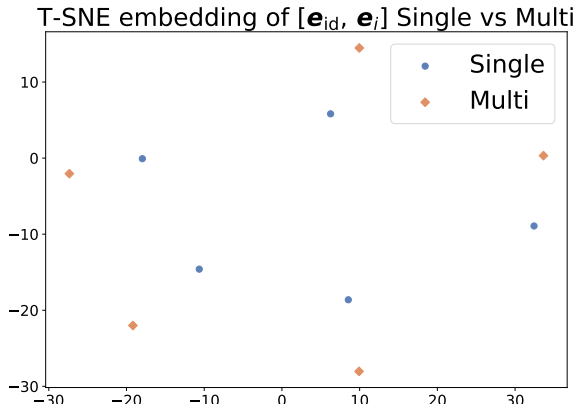
$$\alpha_{\text{exp}} = 0.025, \quad \beta_{\text{exp}} = 1.0, \quad \alpha_{\text{sup}} = -0.01, \quad \beta_{\text{sup}} = 0.05.$$

#### B.4. DiT layer selection

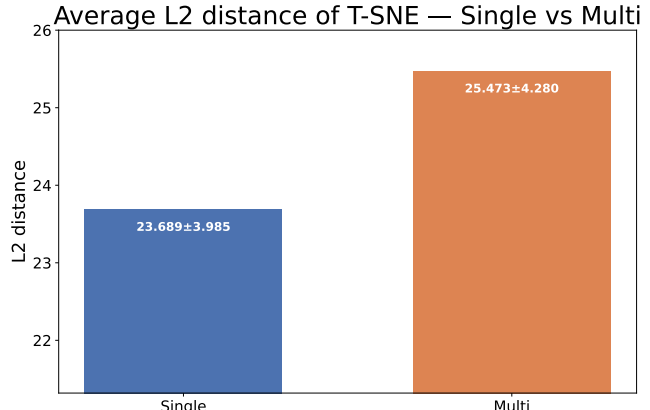
We restrict AFS and STM-based modification to these blocks because prior analyses of FLUX identify them as semantically influential “vital layers.” [2] Modulating only these key layers enables effective identity-aware control while preserving the stability and visual fidelity of the underlying model.

### C. Discriminative criterion for highly ambiguous descriptions

As described in Sec. 3.4, we define the ambiguity level of an identity description. A *high-ambiguity* description indicates that generated images exhibit diverse appearances when conditioned on an identity prompt  $p_{\text{id}}$  combined with multiple per-image prompts  $(p_1, \dots, p_k)$ . Conversely, a



(a) t-SNE comparison of single vs multi prompt embeddings.



(b) Average pairwise  $L_2$  distances of single vs multi.

*low-ambiguity* description indicates consistent character appearances across the prompt set.

To identify transformer blocks and timesteps where ambiguity can be clearly distinguished, we first create distinct high- and low-ambiguity sample sets. We generated 711 prompt sets  $\{p_{id}, p_1, \dots, p_k\}$  using a large language model (ChatGPT), instructed to randomly produce identity and per-image descriptions ranging from simple (e.g., "a zebra") to highly detailed (e.g., "a 16-year-old girl with wavy chestnut hair, a slender frame, and soft brown eyes"). Subjects included animals, people, objects, food, etc., ensuring no overlap with our evaluation set.

We synthesized images from these prompts using a naive diffusion model (FLUX) and measured visual similarity within each prompt set using DreamSim. We labeled the lowest 15% similarity scores as the high-ambiguity set and the highest 15% as the low-ambiguity set, resulting in 107 sets each. The remaining 497 sets were excluded from classification.

We then calculated the mean Euclidean radius of residual features from each transformer block at every denoising timestep, conditioned on each prompt set. Higher mean Euclidean radius indicates widely dispersed samples (high ambiguity), while lower values indicate tightly clustered samples (low ambiguity). We found the most distinctive ambiguity discrimination at transformer block 23 and timestep 4:

- High ambiguity:  $0.1571 \pm 0.0135$
- Low ambiguity:  $0.1032 \pm 0.0116$

The effect size (Cohen's  $d$ ) was 4.26, indicating minimal overlap between the two distributions. Based on these observations, we set an optimal Euclidean radius threshold at 0.1285 for ambiguity classification:

- High ambiguity if mean Euclidean radius  $> 0.1285$
- Low ambiguity if mean Euclidean radius  $\leq 0.1285$

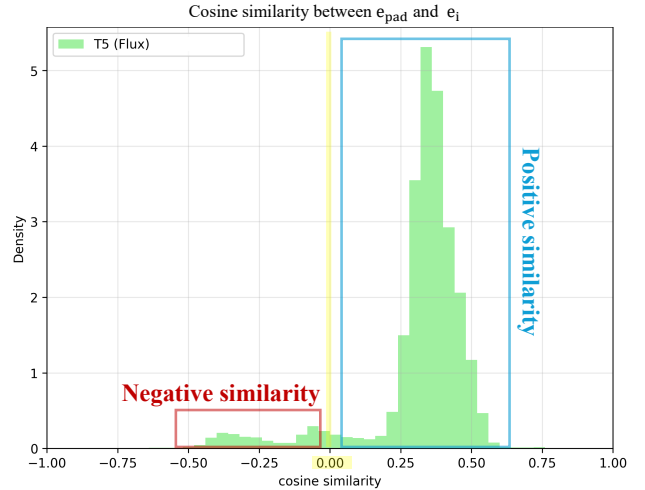


Figure A2. Distribution of cosine similarities between padding embeddings ( $e_{pad}$ ) and embedding  $e_i$ , where  $e_i$  represents either identity embeddings ( $e_{id}$ ) or per-image prompt embeddings ( $\{e_1, \dots, e_k\}$ ). The analysis uses approximately 100 samples from our benchmark.

## D. Semantic Information in Padding Embeddings

In this section, we explain our rationale for adjusting semantic information within padding embeddings, as detailed in Sec. 3.3. As widely recognized [30], the T5 embeddings used for conditioning in FLUX contain fewer semantic details compared to the CLIP embeddings employed by SDXL. However, they still retain some semantic content, although significantly less than CLIP embeddings.

As demonstrated in Sec. 4.2, padding embeddings primarily consist of dummy information but also retain a small amount of meaningful semantic content. Fig. A2 further il-

lustrates that padding embeddings include not only orthogonal (dummy) components but also positive and negative components. Even considering the significant proportion of positive components shared as common vectors in T5 embeddings [12, 21], the existence of negative components indicates that the padding embeddings are not purely orthogonal and irrelevant.

Therefore, we leverage the residual semantic content in T5 embeddings by amplifying semantics relevant to per-image prompts and suppressing irrelevant semantics. This approach, described in Sec. 3.3, repurposes padding embeddings as semantic containers.

## E. Comparison Details

### E.1. Evaluation benchmark

For quantitative evaluation, we introduce a novel text benchmark. Existing benchmarks, such as Consistency, use excessively long identity prompts and relatively short per-image text prompts. Moreover, the detailed style descriptions repeated across all samples often allow the character identity to be inferred directly from the prompt, complicating an accurate evaluation of identity consistency and per-image text alignment.

Therefore, we generated a new benchmark using a large language model (ChatGPT), instructing it with the following criteria:

- Identity prompts should not be overly detailed, allowing diverse interpretations or referencing specific objects (e.g., a cat).
- Per-image text prompts should include variations in pose and background for diversity.
- Style descriptions should constitute approximately 20% of the prompt, emphasizing broad styles such as “cartoon” or “sketch.”

In total, we generated 96 text samples for evaluation.

### E.2. Competitors

We compare our method against several training-free models for consistent identity generation. Below, we detail each competitor’s evaluation setup and notable limitations. All competitors were evaluated using their official repositories.

**FLUX** To determine the scope of identity-consistent generation achievable by the backbone itself, we include FLUX [4], our backbone model, and the current state-of-the-art text-to-image diffusion model. Specifically, we use the FLUX-dev implementation from diffusers.

**Consistency** Consistency [29] generates consistent subjects by injecting features into attention maps based on masked feature correspondences, utilizing an SDXL backbone. Due to its reliance on feature-similarity-based correspondence,

Consistency occasionally generates unrealistic shapes (e.g., a character with three legs). Additionally, being limited to U-Net-based architectures, it struggles with text alignment, falling behind recent diffusion models.

**1Prompt1Story** 1Prompt1Story [22] achieves consistency via text embedding modifications and shared text-attention features. However, it considers only text-level modifications aimed at improving per-text alignment without explicit identity preservation mechanisms. Consequently, when the identity prompt is ambiguous (e.g., “a man”), identity preservation fails. Its reliance on U-Net-based architectures further limits its text alignment capabilities.

**FLUX-kontext** FLUX-kontext [16] generates images reflecting a reference subject and conditional texts. For evaluation, we first generate a reference image using the identity prompt, then produce samples conditioned on per-image text prompts. This approach struggles with variations in poses specified in per-image prompts, often resulting in unrealistic or poorly aligned outputs.

**CharaConsist** CharaConsist [31] ensures character identity by employing RoPE-based feature correspondence in FLUX. This baseline performs well primarily when identity descriptions are detailed enough for FLUX itself to maintain consistency. CharaConsist explicitly requires separate prompts: a Character prompt (appearance), an Environment prompt (background), and an Action prompt (pose). In our evaluation, we directly use our identity prompts as Character prompts and separate Action and Environment prompts from per-image prompts via ChatGPT.

### E.3. Evaluation protocol

**Per-image Text Alignment** For per-image text alignment, we adopt VQAScore [19] with the official code. Following the original protocol, we query the model with the question “Does this image show { }?” and measure the probability that the answer is “Yes”, which serves as the alignment score for each image. We use Qwen2.5-VL-7B-Instruct [3] as a VQA model.

**Identity Consistency** To measure identity consistency across generated images, we calculate perceptual similarity using DreamSim [10]. DreamSim effectively captures semantic content, allowing us to compute similarity scores between all pairs of generated images. The final identity consistency score is obtained by averaging these values across all sample pairs.

	CQS <sub>har</sub> ↑	Per-image text alignment ↑	Identity consistency ↓
(a) FLUX	0.488	0.631	0.429
(b) FLUX + STM	0.541	0.625	0.324
(c) FLUX + STM&PAD	0.543	0.628	0.326
(d) FLUX + AFS	0.500	0.622	0.396
(e) <b>Ours</b>	0.553	0.627	0.302
(f) FLUX + PAD	0.491	0.619	0.408

Table A1. Ablation study comparing the FLUX baseline, STM, STM+PAD, AFS, and our full model, with an additional projected PAD-only variant (FLUX+PAD).

## F. Ablation studies

### F.1. PAD-only Ablation

We additionally include a PAD-only variant (FLUX+PAD) in Tab. A1 to directly compare the effect of projected PAD alone.

- PAD-only improves identity consistency.** Projecting suppress per-image embedding onto padding embeddings slightly improves identity preservation compared to the FLUX baseline, suggesting that padding embeddings can function as a basic semantic register for organizing per-image semantics.
- PAD-only offers only marginal overall benefit.** Despite the improvement in identity consistency, the PAD-only configuration provides only a minor gain in CQS<sub>har</sub> and slightly decreases text alignment. This suggests that naive usage of padding embeddings acts merely as a weak identity regularizer rather than a balanced semantic controller.
- STM+PAD is consistently superior to PAD-only.** When STM is combined with PAD, both identity consistency and text alignment improve. This demonstrates that STM structures expression-related semantics so that PAD embedding serves as an effective semantic register, whereas PAD alone lacks sufficient organization to yield balanced improvements.

### F.2. Qualitative results of ablation settings

Fig. A3 illustrates the qualitative results of each ablation setting:

- The FLUX baseline generates inconsistent identities across frames (See A1~A4).
- Adding AFS alone produces limited improvement in identity preservation(See B1~B3).
- Using only PAD improves identity consistency (A2 → D2, A4 → D4) to a limited degree but remains insufficient (D1~ D3).
- Using only STM also shows clear limitations in maintaining identity. (See C1→ C3)
- Combining STM and PAD results in significantly better identity preservation.(D2 → E2, D4 → E4)

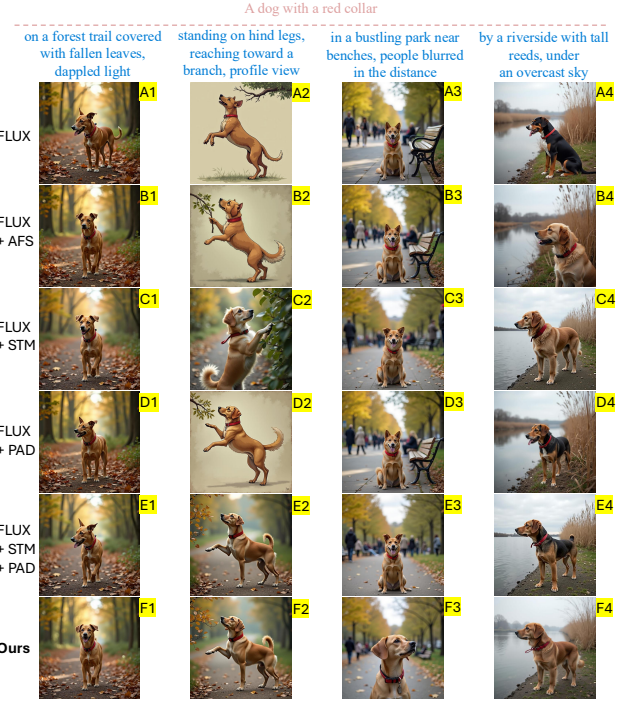


Figure A3. Qualitative results of ablation settings.

- Adding AFS on top of STM+PAD (**Ours**) further improves identity consistency while maintaining strong text alignment. (See F1~F4)

## G. Stability of CQS and robustness of model performance

$\mu, \tau$	Ours	Flux Kontext	FLUX	CharaConsist	Consistency	IPrompt1Story
0.1	<u>0.5670</u>	0.5463	0.5045	0.4585	0.4406	0.2692
0.2	<u>0.5642</u>	0.5449	0.5013	0.4554	0.4377	0.2670
0.3	<u>0.5610</u>	0.5432	0.4976	0.4520	0.4343	0.2646
0.4	<u>0.5574</u>	0.5413	0.4933	0.4480	0.4306	0.2619
0.5	<u>0.5533</u>	0.5390	0.4885	0.4436	0.4264	0.2588
0.6	<u>0.5491</u>	0.5365	0.4834	0.4389	0.4217	0.2556
0.7	<u>0.5444</u>	0.5337	0.4780	0.4341	0.4164	0.2523
0.8	<u>0.5393</u>	0.5305	0.4721	0.4292	0.4107	0.2486
0.9	<u>0.5343</u>	0.5269	0.4661	0.4241	0.4046	0.2446
1.0	<u>0.5291</u>	0.5230	0.4603	0.4192	0.3997	0.2407

Table A2. CQS<sub>har</sub> comparison across different reward and penalty weights ( $\mu, \tau$ ). Our method consistently achieves the best score, followed by the second-best underlined.

### G.1. Effect of weighting on CQS stability.

This subsection analyzes the sensitivity of the proposed Consistency Quality Score (CQS<sub>har</sub>) to variations in the reward and penalty weights  $\mu$  and  $\tau$ . As shown in Tab. A2, we jointly vary both weights from 0.1 to 1.0 to examine the stability of the metric across a wide range of configurations. Across all settings, our method consistently achieves

the highest  $CQS_{har}$  values, while FLUX consistently ranks lowest among the baselines. As  $\mu$  and  $\tau$  increase, the influence of balance regularization is amplified, causing models with weaker trade-offs between identity consistency and text alignment, such as FLUX and Consistency, to exhibit faster score degradation. Importantly, the relative ranking of models remains unchanged across all weight configurations, confirming that  $CQS_{har}$  robustly emphasizes balanced generation and provides stable and discriminative model ordering even under large variations in weighting.

## G.2. Robust performance of our method.

Our method exhibits strong robustness to increasing balance penalties, maintaining stable performance while consistently outperforming all baselines under the  $CQS_{har}$  metric. While FLUX and Consistency [29] show a steep decline in  $CQS_{har}$  as the weights increase, with their scores dropping from 0.504 to 0.460 ( $\Delta = 0.044$ ) and from 0.441 to 0.400 ( $\Delta = 0.041$ ), respectively, our method remains remarkably stable across all weighting conditions. Specifically, the overall CQS score of our method decreases only slightly, from 0.567 to 0.529 ( $\Delta = 0.038$ ), corresponding to a mild 6.7% reduction despite the increased penalty strength. Moreover, the relative performance gaps remain highly consistent across the entire range: the margin between our method and the FLUX baseline exceeds 0.06 in all cases, while the gap to Flux Kontext [16] remains around 0.022.

## H. Limitations

In this section, we discuss the limitations of our framework. Our approach preserves identity mainly through text-based adjustments and residual feature sharing. However, it struggles to achieve high-fidelity identity consistency when the identity prompt describes natural scenes or food, such as “a lush mountain range.”

This limitation arises from our adaptive residual feature-sharing strategy. Residual features encode character-level shape identity only implicitly [15]. When the identity prompt instead represents nature or food, these residual features no longer contain information sufficient to define a coherent identity. Moreover, even our ambiguity-aware distinctiveness metric fails to clearly distinguish high-ambiguity from low-ambiguity samples under these conditions, since it relies on the coherence of residual features.

Thus, an alternative strategy beyond adaptive feature sharing is required in these cases, which we leave for future work.

## I. More qualitative comparison sample

We provide more qualitative comparison sample in Fig. A4,

Fig. A5, Fig. A6, Fig. A7 and Fig. A8.

### A parrot

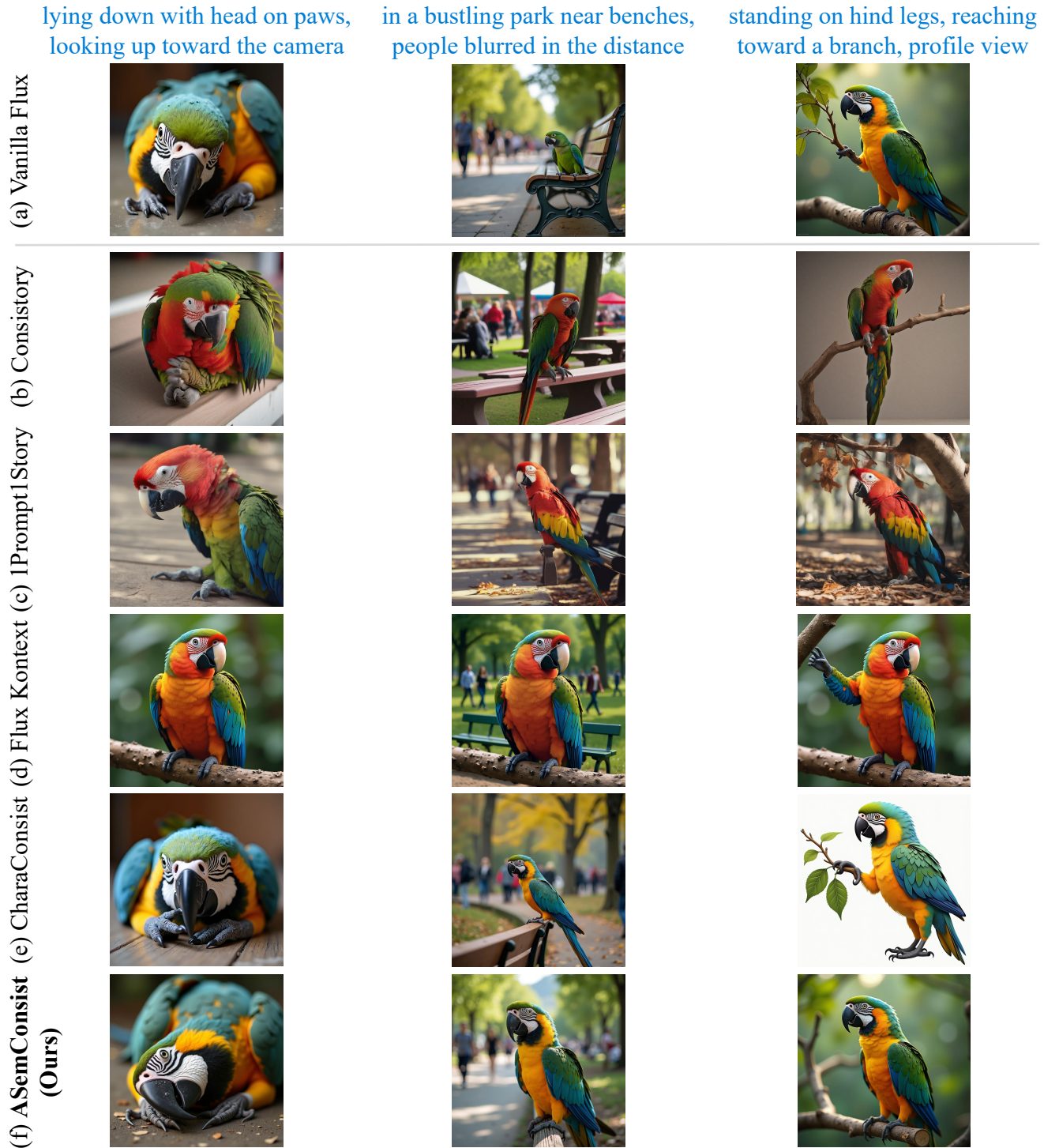


Figure A4. Qualitative comparison

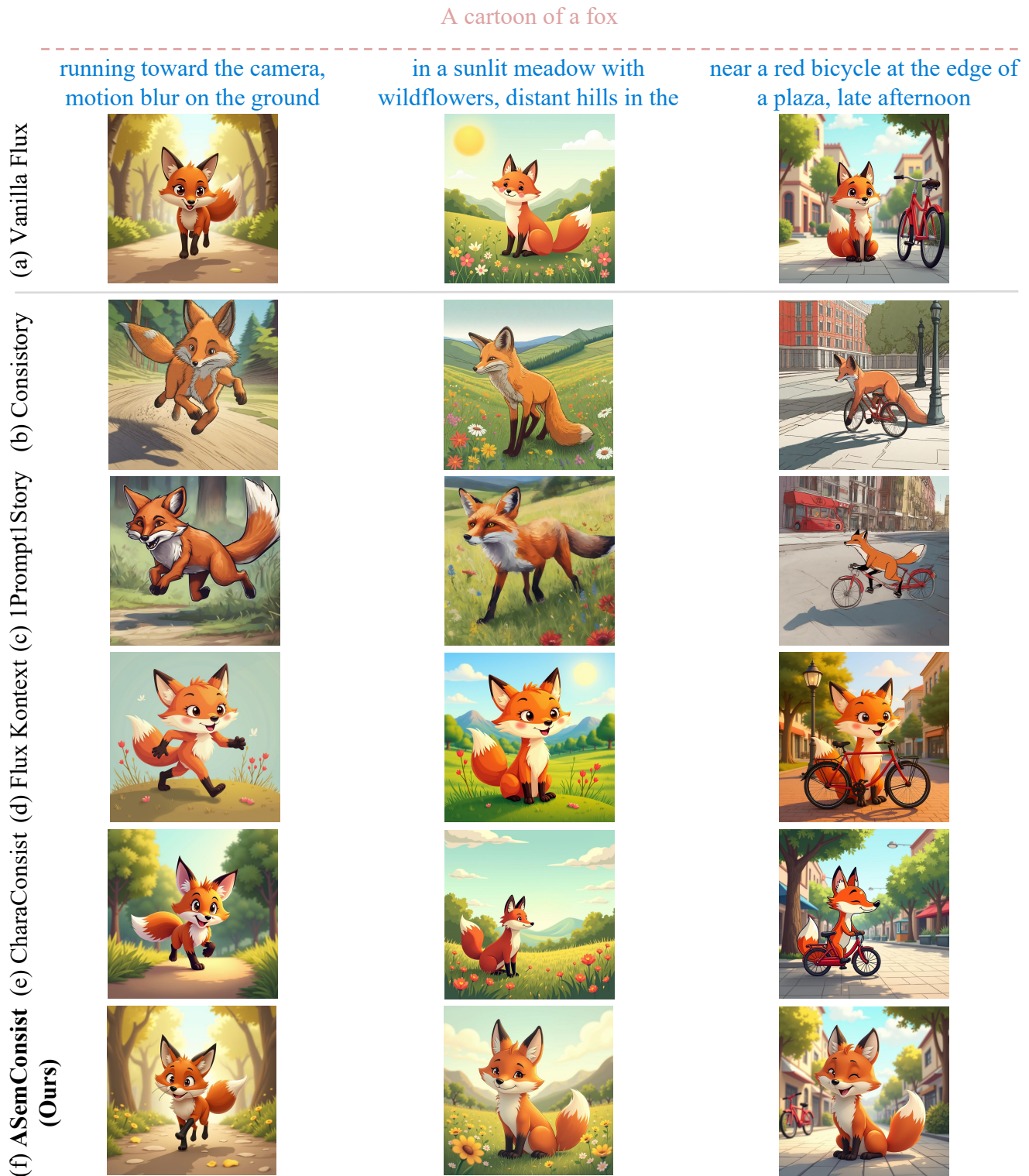


Figure A5. Qualitative comparison

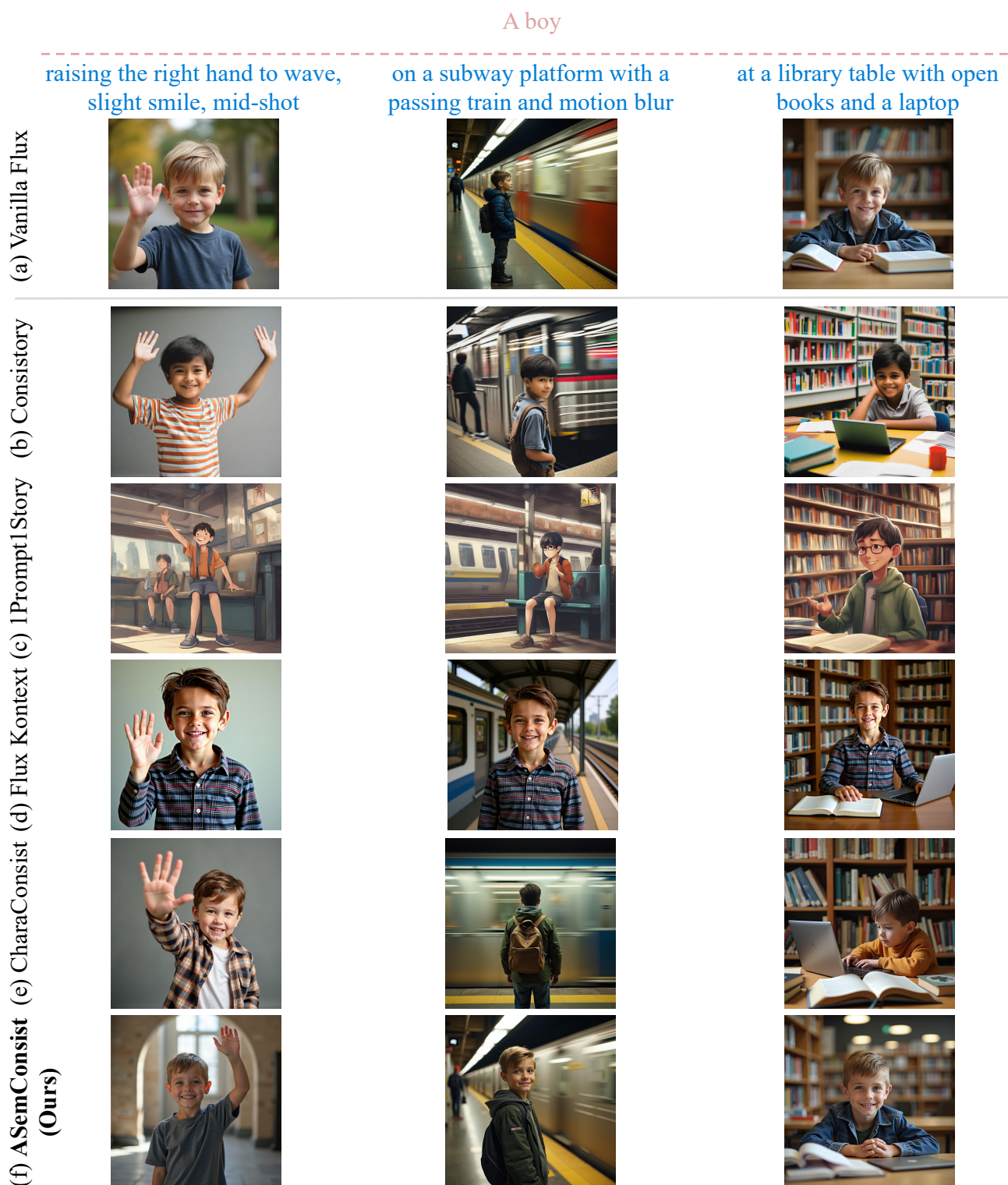


Figure A6. Qualitative comparison

A sketch of An elderly woman wearing a lanyard

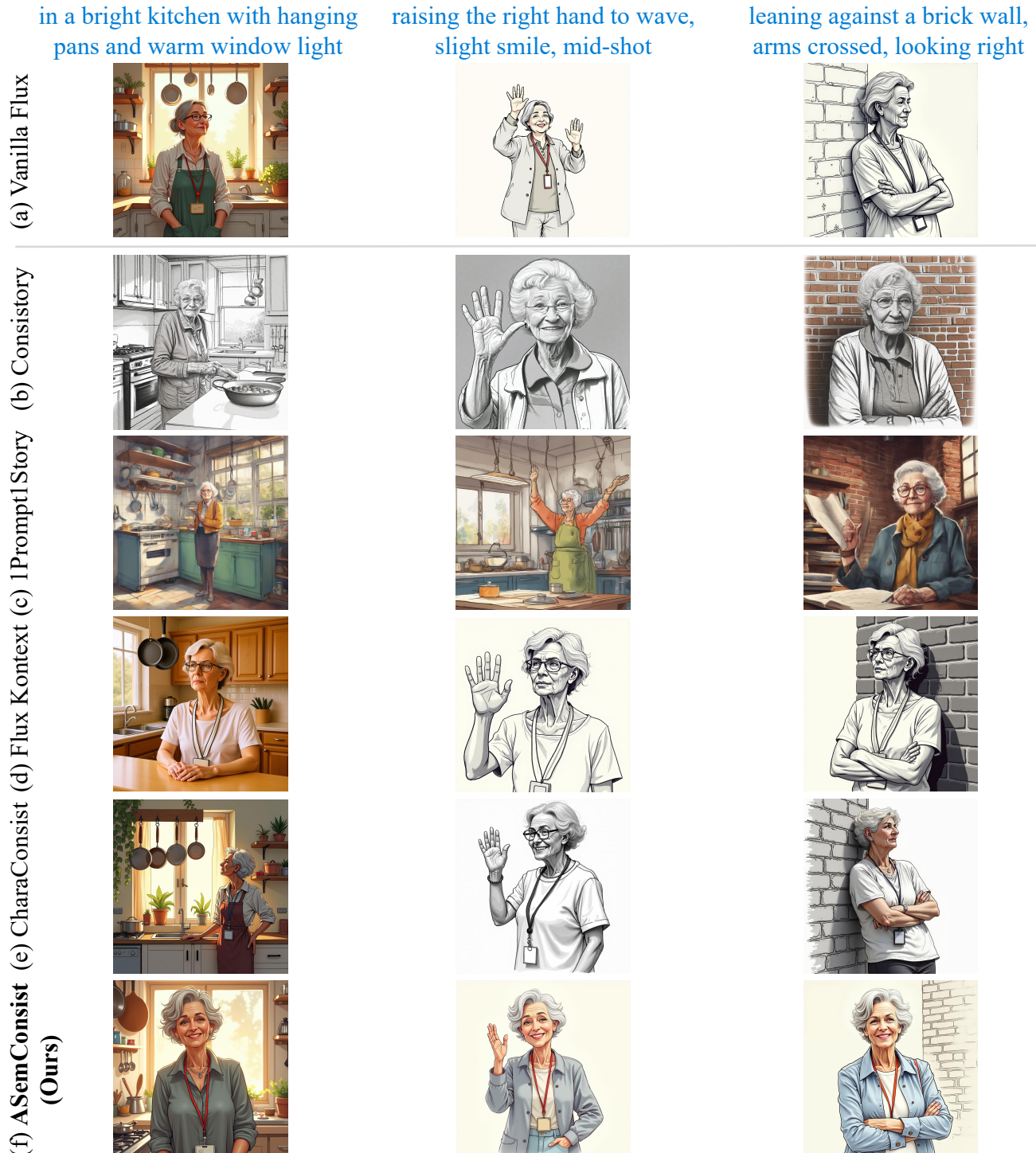


Figure A7. Qualitative comparison



Figure A8. Qualitative comparison